38th Fluid Dynamics Conference and Exhibit
23 - 26 June 2008, Seattle, Washington

AIAA 2008-4169

Unsteadiness Characterization in a Shock Wave Turbulent Boundary Layer Interaction through Dual-PIV

Louis J. Souverein[1]
Institut Universitaire des Systèmes Thermiques Industriels, Marseille, France

Bas W. van Oudheusden[2] and Fulvio Scarano[3]
Delft University of Technology, Delft, the Netherlands

and

Pierre Dupont[4]
Institut Universitaire des Systèmes Thermiques Industriels, Marseille, France

The unsteady organization and temporal dynamics of the interaction between a planar shock wave impinging on a turbulent boundary layer at a free stream Mach number of M_∞=1.69 is investigated experimentally by means of dual-plane Particle Image Velocimetry (dual-PIV). Two independent PIV systems were combined in two component mode to obtain instantaneous velocity fields separated by a prescribed small time delay. This enables to obtain, in addition to mean and statistical flow properties, also instantaneously time resolved data to characterize the temporal dynamics of the flow phenomenon in terms of time scales, temporal correlations and convective velocities. The characteristic time scales for the incoming boundary layer, the separation region and the reflected shock are evaluated by means of measuring the temporal auto-correlation coefficient in the complete flow field for a range of time delays from 5 μs to 2000 μs. These auto-correlation fields are used to quantify the time scales in selected regions of the flow. This permits resolving the dominant time scales within the boundary layer and the interaction region.

I. Introduction

The effect of a planar shock impinging on a turbulent boundary layer establishes one of the classic interaction phenomena in compressible viscous flow analysis. This particular form of interaction has also direct technological relevance to the performance of high speed vehicles, affecting notably the efficiency of supersonic intakes. Furthermore, maximum mean and fluctuating pressure and thermal loads on a structure are most often found in regions of shock wave boundary layer interaction (SWBLI) and are thus important factors in vehicle development. Flow control is seen as an important issue in future vehicle design (see Ref. 2). The renewed attention for the feasibility of sustainable supersonic transport has revived the interest in SWBLI in the moderate supersonic regime. In this context the European sixth framework program UFAST "Unsteady effects in shock wave induced separation" was recently initiated, in which the shock reflection interaction is one of the flow cases of interest.

Conventional two-component PIV measurements have been performed to investigate the statistical and instantaneous behavior of shock wave boundary layer interactions (see for example Ref. 10). Although these measurements give a good idea of the overall flow organization, information is lacking on its temporal development, as characterized by instantaneous quantities like time scales, characteristic frequencies and the local acceleration. Knowledge of these quantities would profoundly increase the understanding of the flow, especially considering the correlation between events in different regions of the flow. One can think of the relation between the motion of the reflected shock and upstream and downstream events (respectively the passage of turbulent structures through the

[1] Research Assistant, Groupe Supersonique, 12 Avenue Général Leclerc, F-13003 Marseille, AIAA Member.
[2] Associate Professor, Faculty of Aerospace Engineering, Kluyverweg 1, NL-2629 HS Delft.
[3] Associate Professor, Faculty of Aerospace Engineering, Kluyverweg 1, NL-2629 HS Delft.
[4] Chargé de Recherche, Groupe Supersonique, 12 Avenue Général Leclerc, F-13003 Marseille, AIAA Member.

interaction and the expansion and contraction of the separation bubble), see Refs. 2, 5 and 9. Furthermore, the local acceleration field would permit compressible loads determination methods as discussed in Refs. 15, 19 and 16 to be extended to include instantaneous loads and pressures (see Ref. 11). However, due to the technical restrictions on both the double pulse repetition rate of the laser system and the acquisition rate of the cameras, the recording frequency is limited to 10 Hz for conventional PIV systems, and still to typically a 1-10 kHz for currently available high-speed PIV systems (at a strong reduction of image quality in terms of illumination power and spatial resolution). This is by far insufficient to obtain accurate time-resolved data for this high speed flow case under investigation. The time scales in shock wave turbulent boundary layer interaction typically span three orders of magnitude[3]: O(10 kHz) for the incoming boundary layer, O(1 KHz) for the mixing layer developing inside the interaction and O(100 Hz) for the reflected shock motion. For example, for the flow under consideration the integral time scales in the incoming boundary layer are estimated at 24 µs, the associated frequency being 42 kHz (see section V).

To study the interaction with sufficient temporal resolution, two independent PIV systems were therefore combined to obtain instantaneously time resolved whole field measurements, where the time delay between the acquisitions from both PIV systems could be set to arbitrarily small values, not limited by the repetition-rate restrictions of a single system. This way time correlated data could be obtained as well as acceleration data. The advantage of this approach with respect to the current state of the art time-resolved PIV systems is in the first place the higher laser power and image resolution. Secondly, it allows setting the delay time between the two PIV systems independent of the pulse separation of the individual systems, as well as to realize very small delay times. The smallest time separation employed in the current investigation was 5 µs, corresponding to an effective frequency of 200 kHz (as opposed to acquisition rates in the order of 1 kHz for available high-speed PIV systems). This allows temporally resolving the time scales within the boundary layer and within the interaction region.

Presented here are the results obtained with this Dual-PIV system. In the first place the system itself is discussed. Secondly, the quality and consistency of the Dual-PIV measurements is discussed, and the data is validated by means of a comparison to available boundary layer data, semi-empirical relations and earlier SWBLI measurements. Thirdly, an overview is given of the obtained mean and fluctuation statistics. Finally, the temporal auto-correlation coefficients are obtained for the complete flow domain and different delay times, yielding characteristic time scales for different regions in the flow, specifically for the reflected shock, the incoming boundary layer and the separation zone.

II. Experimental Arrangement

The experiments were performed in the TST-27 transonic supersonic wind tunnel of the High-Speed Aerodynamics Laboratory at Delft University of Technology, with test section dimensions of 280 mm (width) × 270 mm (height). It is a blow-down facility that can operate at Mach numbers ranging from 0.5 to 0.85 and from 1.15 to 4.2 and a unit Reynolds number of 30×10^6 to 130×10^6 m^{-1}, with a run time of up to 300 s. The Mach number is set by means of a continuously variable throat and flexible upper and lower nozzle walls. The stagnation pressure can be set independently with typical values in the range of 2.0 to 3.0 bar, the stagnation temperature is determined by the outside temperature. The velocity transient inherent to blow down operation has been determined to be approximately 5×10^{-2} m/s^2 corresponding to a total temperature transient of 6×10^{-2} K/s. The effect on the mean velocity is less than 1% of the free-stream velocity over a complete run duration of 60 seconds.

During the current measurement campaign, test were performed at a nominal free stream Mach number of M_∞=1.69 (U_∞=448 m/s), a total temperature of T_0=273 K and a total pressure of p_0=2.3 bar resulting in a free stream unit Reynolds number of 36×10^6 m^{-1}. The thickness of the boundary layer is approximately δ_{99}=17.2 mm. The boundary layer was assessed to be in fully developed turbulent condition with a Reynolds number based on momentum thickness of approximately 50,000. The incident shock wave for the SWBLI was generated by a full-span wedge imposing a flow deflection of 6.0° (see figure 1). The shock generator was mounted such as to position the interaction region in the centre of the field of view, as well as to postpone the interaction of the expansion fan emanating from the shoulder of the wedge with the recovering boundary layer (the estimated point of impact is 3δ behind the shock intersection point). A stable and reproducible flow was achieved over both sides of the wedge even at the relatively low Mach

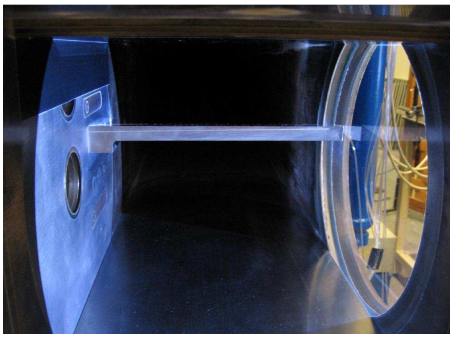

Figure 1: Experimental configuration

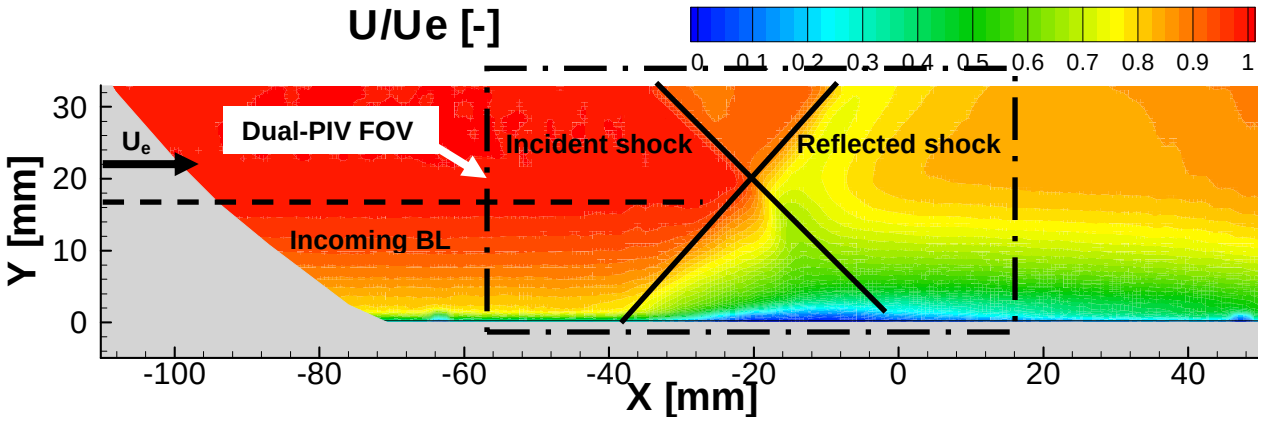

Figure 2. Panoramic field PIV measurement of the SWBLI under consideration.

number. The flow topology of the SWBLI under consideration can be seen in figure 2. Shown are the incoming boundary layer, the incident shock and the reflected shock, and the selected field of view of the Dual-PIV measurements. The gray area indicates the wall and the edge of the optical access. The flow is from left to right.

A Dual-PIV system was set up to acquire the locally time resolved PIV data to obtain time correlated velocity field information. Illumination is provided from downstream of the test section wile the observation is performed through a large window in the sidewall. The principle op Dual-PIV depends on the mutually independent operation of two two-component (2C) PIV systems. Both systems are aligned to provide illumination in the same measurement plane while observing identical fields of view, see figure 3. The laser light of the two systems was optically separated by means of polarization and the beams of the two lasers were combined and aligned before entering into the light sheet optics. The overlap of the field of view of both cameras was guaranteed by means of a polarizing beam splitter cube, which also assured the independence of the two PIV systems by separating the images based on the polarization. Both cameras were equipped with an additional polarizing filter to further improve the independence.

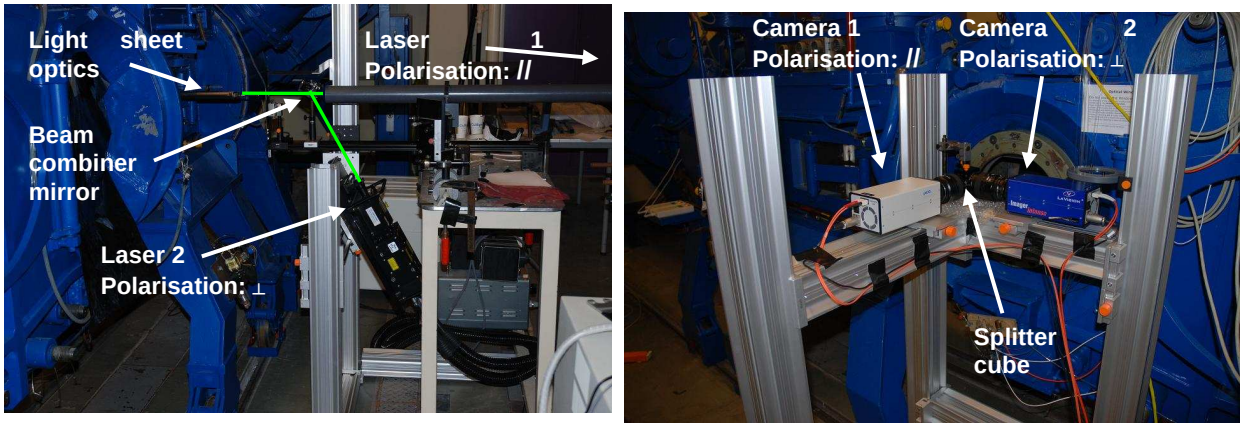

Figure 3. Experimental arrangement; left: setup of the lasers with beam combiner; right: setup of the cameras with splitter cube.

Care was taken that the total of four laser sheets generated by both laser overlapped in space. Furthermore, special attention was dedicated to the temporal alignment of the laser pulses. The triggering was calibrated such that both lasers flashed simultaneously for a zero time delay between both systems (δt_2=0 µs), see figure 4 for the timing diagram. This was done by means of a calibration run, determining the temporal off-set in the Q-switch trigger between both lasers through a correlation of the images corresponding to the respective laser pulses (i.e. image 1A with image 2A).

Particular attention was given to the alignment of the FOV of both cameras. The alignment of the cameras was accessed by means of the displacement field obtained for δt_2=0 µs and zero flow velocity (no airflow through the

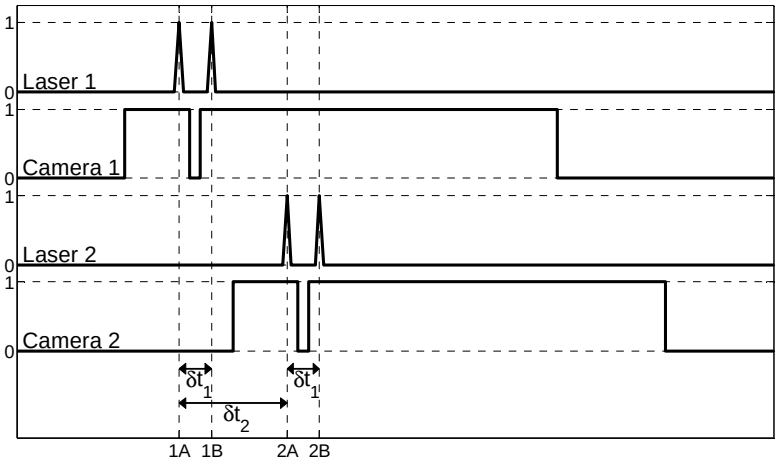

Figure 4. Dual PIV timing diagram.

tunnel). The corresponding homogeneous deformation was obtained in terms of the dilatation, the rotation and the translation components. This analysis shows that the difference in magnification and rotation between the two FOVs is negligible: the difference in magnification is in the order of 0.1 % and the rotation is in the order of 10^{-2} degrees. The horizontal and the vertical mismatch between the FOVs are in the order of 1 pixel, which is small as compared to the interrogation window size (31 x 31 pix). It is therefore concluded that the alignment of the cameras was made to such a degree of accuracy that an image dewarp is not required (more details can be found in Ref. 16).

The potential of the current setup becomes evident from the timing-schematic in figure 4, since for a given pulse-delay δt_1, the time separation δt_2 can be set arbitrarily (and indeed even δt_1 for each PIV system individually as well, if desired). This allows obtaining time correlated data at different time scales. In theory, measurements can be made with an unlimited temporal dynamic range, since δt_2 can be set to any value between zero and infinity. In the current experiment, as sweep of δt_2 was performed in the range of 5 µs to 2000 µs (corresponding to a equivalent frequencies of 200 kHz to 0.5 kHz) with a reference measurement at 0 µs. to check the consistency between the two PIV systems. A minimum of 200 acquisitions (400 image pairs) were made per time delay.

The illumination was provided by a Spectra-Physics Quanta Ray laser (400 mJ/pulse energy and a 6 ns pulse duration) and a Quantel laser (300 mJ/pulse energy and a 9 ns pulse duration), installed as lasers 1 and 2 respectively. Both are double-pulsed Nd:Yag laser with a wavelength of 532 nm. The light sheet thickness was approximately 2 mm. The flow was seeded with DEHS droplets with an estimated effective particle size of about 1 micron dispersed in the settling chamber of the wind tunnel. The particle images were recorded at 12-bit with a resolution of 1376 × 1040 pixel using a PCO Sensicam QE (camera 1) and a LaVision Imager Intense QE (camera 2), both equipped with a Nikon f=60mm lens, diffracting with $f_{\#}$=8. Of the CDDs only 992 pixels were used in the vertical direction given the aspect ratio of the interaction region of interest. The flow was imaged over a FOV of 76 mm x 55 mm (approx. $4\delta \times 3\delta$) in streamwise and wall-normal direction respectively, at a digital resolution of 55.1 µm/pixel. The timing and data acquisition was performed by Davis 7.2 in combination with a PTU 9 timing unit.

Recordings were made at an acquisition rate of 5 Hz. The pulse separation δt_1 was kept constant to 1.5 µs for both laser systems, producing particle displacements of approximately 0.7mm (corresponding to 12 pixels) in the free-stream flow. The image pairs were interrogated using the WIDIM algorithm[13], employing correlation window deformation with an iterative multi-grid scheme, at 31×31 pixels window size (1.7 mm x 1.7 mm) and an overlap factor of 75%. This resulted measurement grid resolution is 0.43 mm and 0.43 mm in *x* and *y* direction, respectively.

III. Data validation

Since the field of view is identical, the velocity statistics obtained from each PIV system should be identical to within the statistical convergence error. As has been verified previously[16] the results obtained from each individual system is identical to within the statistical convergence and no significant effect of the inherent camera alignment uncertainty on the mean and fluctuation statistics was observed.

To further evaluate the measurement quality, a validation of the flow data is performed based on the incoming boundary layer profile and the statistical profiles within the interaction region. The data has also been compared to additional two-component PIV measurements of the same flow under identical measurement conditions, but at different spatial resolutions, see figure 5. The properties of the reference PIV measurements are summarized in table 1 (Dual-PIV characteristics repeated for completeness). This validation is performed for the complete Dual-PIV data ensemble, encompassing all acquisitions for both cameras combined in the statistical analysis (in total 4000 realisations) as an assessment of the quality of the Dual-PIV measurements.

Table 1: Reference PIV measurement properties

Dataset	*Short name*	*Ensemble size*	*Field of view [-]*	*Digital resolution [μm/pix]*
Dual-PIV	Dual	4000	$4\delta \times 3\delta$	55.1
Panoramic FOV	Pano	700	$9\delta \times 2\delta$	70.1
Boundary layer zoom	BL Zoom	250	$0.7\delta \times 0.9\delta$	11.7
Interaction zoom	Zoom	870	$2.2\delta \times 1.6\delta$	29.0

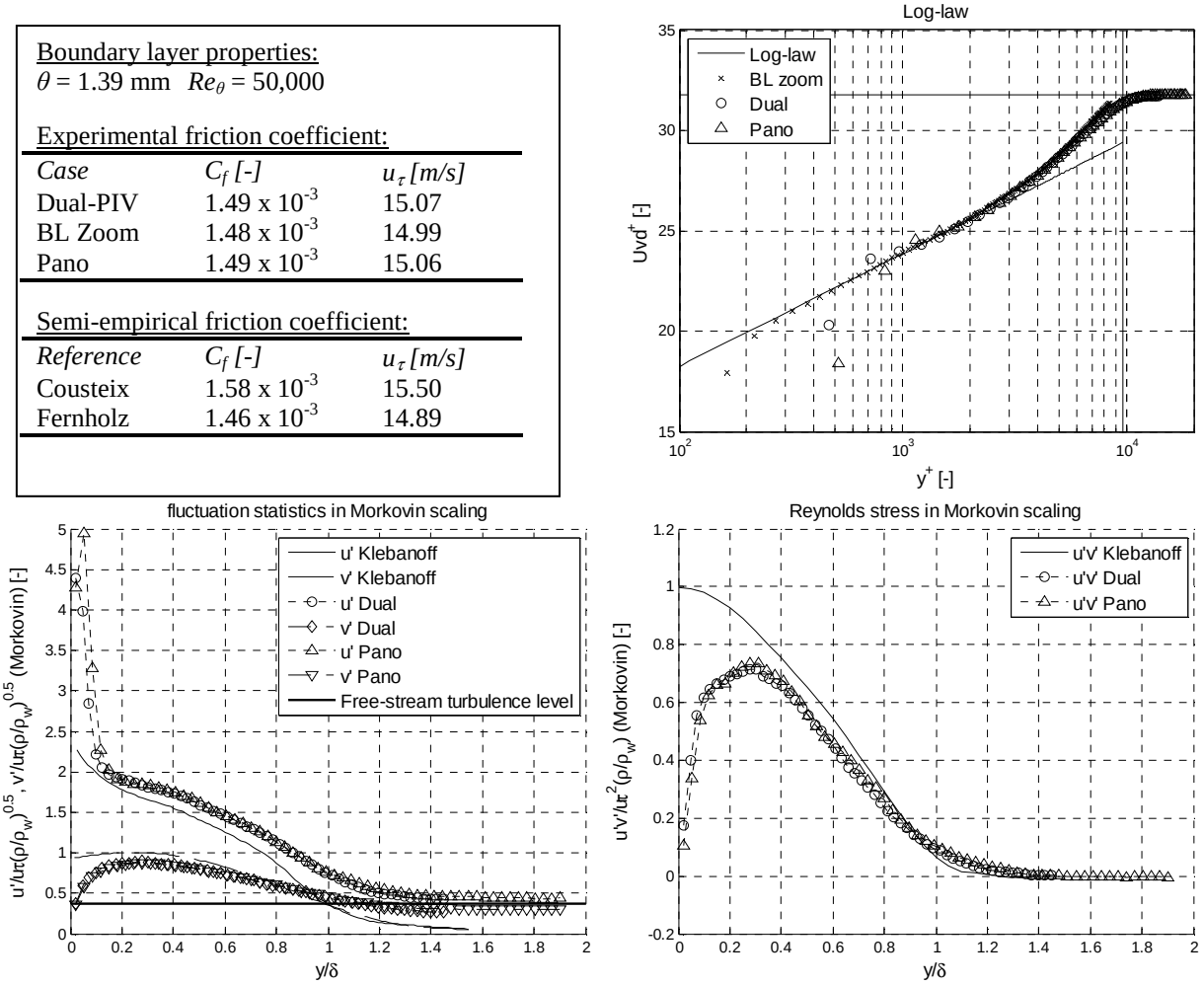

Figure 5: Boundary layer statistics (top-right: log-law of the wall; bottom-left: σ_u and σ_v in morkovin representation compared to Klebanoff reference data; bottom-right: -<*u'v'*> in Morkovin representation compared to Klebanoff reference data.

For the boundary layer profiles, the ensemble size has been augmented by taking statistics in flow direction (over 0.7δ for the boundary layer zoom experiments, 0.6δ for the Dual-PIV data, and 1.5δ for the panoramic measurements) to increase the convergence and to attenuate measurement noise. It has been verified that this does not bias the results. A consistency check has been performed of the friction coefficient and friction velocity obtained from a log-law fit with respect to results from semi-empirical relations (Cousteix, see Ref. 1, and Fernholz, see Ref. 8). As can be observed from figure 5, none of the datasets resolves the log-law down to the viscous sub-layer. This a consequence of the limited PIV-resolution in combination with the high Reynolds number: y^+=30 corresponds to 53 μm, which equals one pixel at the Dual-PIV magnification. The first reliable velocity measurement in the current experiment is at y/δ=0.1, or y^+=1000 (corresponding to one interrogation window size). The velocity fluctuations are in good agreement with the Klebanoff reference data (note that the horizontal line in figure 5 indicates a 1%

turbulence intensity in the free-stream). The u-component fluctuations is resolved with good confidence down to y/δ=0.1. The Reynolds stresses show a reasonable agreement with the Klebanoff profile down to y/δ=0.3. Below this height the stresses are underestimated, which may imply that the Reynold stress measurements near the wall suffer from a systematic measurement error. However, the Dual-PIV measurements are consistent with the earlier experiments. The friction coefficient and friction velocity, see the text box with figure 5, are found to be in good agreement with both the earlier measurements and the semi-empirical correlations. The log-law fit was made without a priori fixing the second constant C. The best fit was obtained for C=7 and u_τ=15 m/s.

Finally, the obtained mean and fluctuating velocity profiles, as well as the Reynolds stress profiles, are compared to the panoramic FOV and interaction zoom PIV measurements at larger (Zoom) and smaller magnification factors (Pano), see table 1. This validation is again performed for the complete Dual-PIV data ensemble. Figure 6 shows the statistical profiles at different stations within the interaction region. The corresponding coordinates of the stations are given in figure 6 (profiles 1 to 5, numbered from left to right, coordinates with respect to extrapolated incident shock foot, section names indicative of approximate location). It can be observed that a very good agreement is

Table 2: Interaction profile stations

Section	*Incoming BL*	*Reflected shock foot*	*Shock crossing*	*Separation bubble*	*Incident shock foot*
Profile no.	1	2	3	4	5
Coordinate [mm]	-50	-30	-20	-10	0

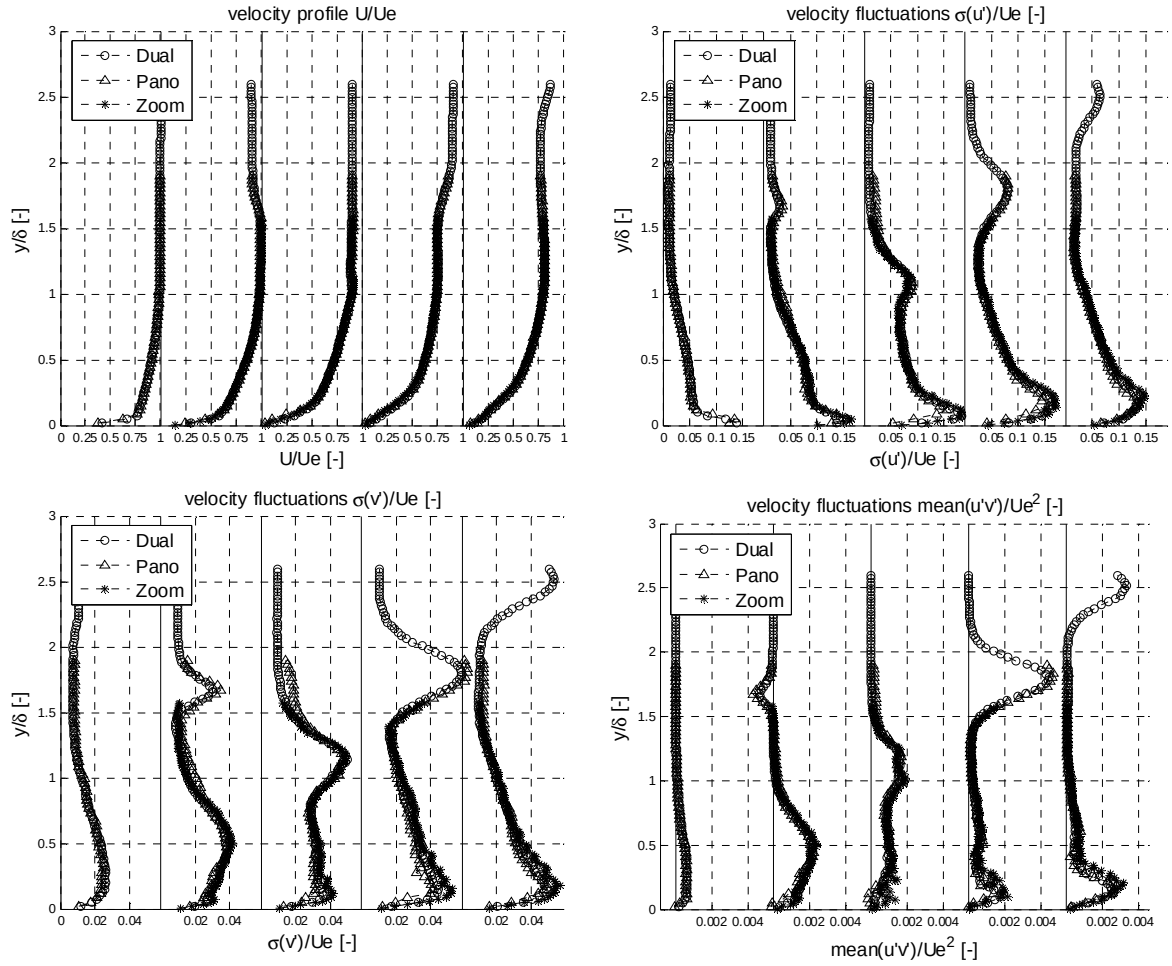

Figure 6: Comparison of statistical profiles within the interaction region (top-left: mean velocity, top-right: σ_u/U_e, bottom-left: σ_v/U_e, bottom-right: $-\langle u'v'\rangle/U_e^2$.

obtained for the mean velocity profiles. Some dispersion is observed for the v-component fluctuation statistics and the Reynolds stresses. This can however be attributed to statistical convergence uncertainties.

In summary, the Dual-PIV boundary layer measurements are found consistent with the earlier measurements and the obtained friction coefficient and friction velocity are in good agreement with the results obtained with the semi-empirical relations. Furthermore, apart from the measurement points close to the wall, no dependence of the flow quantities on the spatial resolution was observed. It may thus be concluded that the datasets are of consistent quality and further that the incoming boundary layer under consideration is a canonical turbulent boundary layer.

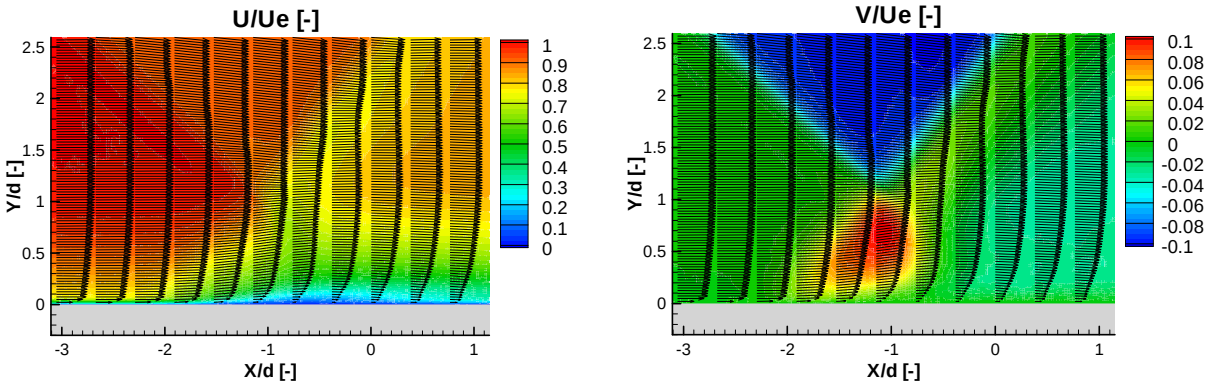

Figure 7. Mean velocity fields; left: u-component, right: and v-component. Statistics based on 4000 acquisitions. Spatial coordinates normalised by the boundary layer thickness (*d*). Origin taken at the extrapolated incident shock foot.

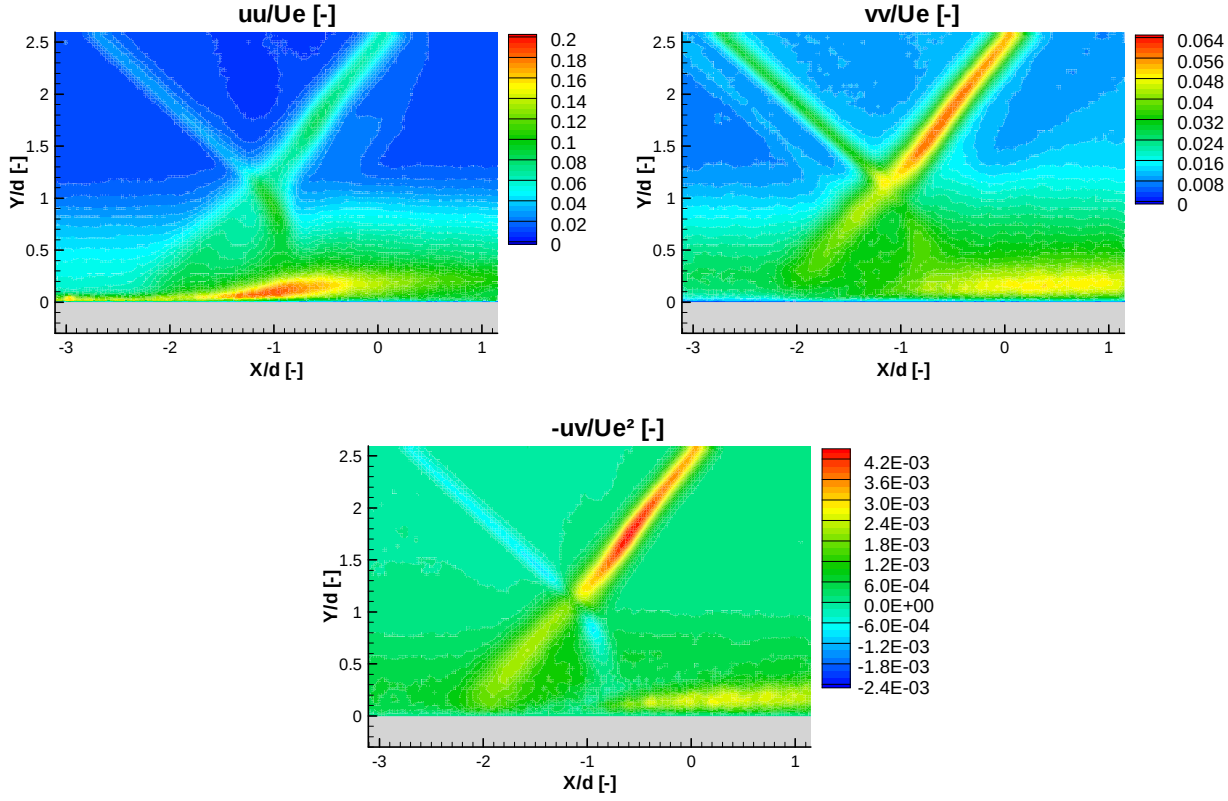

Figure 8. Fluctuation statistics and Reynolds stress; top left: σ_u/U_e; top right: σ_v/U_∞; bottom: $-\langle u'v'\rangle/U_e^2$ Statistics over 4000 acquisitions. Spatial coordinates normalized by the boundary layer thickness (*d*). Origin taken at the extrapolated incident shock foot.

IV. Mean and fluctuation statistics

Figure 7 and figure 8 show the mean velocity field and the fluctuating velocity statistics respectively, providing a global understanding of the flow topology under consideration. The thickness of the undisturbed boundary layer is approximately δ_{99}=17 mm. The interaction length based on the distance between the extrapolated point of impact of the incident shock and the reflected shock foot is approximately 2δ. The figures show that the incoming boundary layer remains undisturbed within at least the first 10mm (0.6δ) of the FOV. The incident shock wave was observed to be stationary and the local velocity fluctuations observed are mainly attributed to PIV measurement uncertainties in the direct vicinity of the shock. The reflected shock shows strong velocity fluctuations as a consequence of pronounced variations in the shock positions. The extent of the reflected shock excursions is estimated, based on the vertical velocity component fluctuations, as approximately ±5mm. Both shocks are smoothed in the mean velocity fields due to a combination of particle inertia, optical refraction effects[7] and the limited PIV spatial and temporal resolution (due to central differencing over the time separation δt_1 between the image pairs). The line of increased v-component fluctuations observed upstream of the incident shock is also due to an optical refraction effect, probably due to the interaction of the shock with the boundary layer on the tunnel window. The particle images in this region are blurred with no physical change in the flow velocity.

Considering the external flow outside the boundary layer, it can be seen that the flow is initially parallel to the wall and consecutively decelerated by the shock system. The first (impinging) shock causes a downward deflection resulting in a negative vertical velocity of approximately -50m/s or about 11% of the free-stream velocity. The second (reflected) shock causes an upward deflection, which is directly followed by an acceleration caused by the expansion fan (which is the actual physical reflection of the incident shock wave). The expansion fan is practically attached to the reflected shock and deflects the flow to a small negative vertical velocity component of approximately -10m/s or 2% of the free-stream velocity. Considering the boundary layer, the strong adverse pressure gradient imposed by the shocks causes it to thicken dramatically and driving it towards separation. However, even though a large region of slow moving fluid exists close to the wall and flow reversal occurs instantaneously, the flow was not observed to be separated on the mean. An increase in the velocity fluctuations and the Reynolds stresses throughout the interaction region can be observed. The large increase in the u-component fluctuations directly behind the reflected shock foot is a consequence of the pulsation of the instantaneous separation bubble. The large u-component fluctuations and the increase in v-component fluctuations and Reynolds stresses are associated to vortical structures developing within the shear layer. Anisotropy can be observed between the stream wise and lateral fluctuation component since the maximum value attained by σ_u is about four times higher than the value attained by σ_v. On the contrary, the u-fluctuation recovers much faster than the v-fluctuation, which is seen to persist until the end of the observation domain.

Based on the above observations, the flow under consideration likely presents the case of an incipient separation on the mean. Nevertheless, instantaneous occurrences of significant flow reversal (separation) have been observed, giving evidence of the important temporal dynamics governing the interaction even for this mild interaction strength. Although the range of dynamic excursions in the instantaneous flow organization may already be appreciated from an ensemble of uncorrelated flow realizations, obtained with a low repetition rate measurement system (see e.g Ref. 10) this does not permit to quantify the dynamics in temporal terms. The aim of the current investigation is therefore to deduce and quantify the time scales of the different aspects in the flow (incoming boundary layer, reflected shock motion, separation region pulsation, shedding of vortical structures).

V. Determination of time scale

Since measurement were performed for a range of time separations from δt_2=0 µs to 2000 µs, this allows time correlation data for the complete flow field to be obtained as a function of the time delay. This can then be exploited to determine the characteristic time scale at each position in the flow. Specific regions of interest are the incoming boundary layer, the recirculation region where vortex production and shedding occurs, the reflected shock, and the recovering boundary layer. Figure 9 and figure 10 show the time correlation coefficient for the u-component of velocity, for small and large time delays respectively, given by Eq.(1), where u'_i is the fluctuation component and σ represents the standard deviation. Furthermore, the indices 1 and 2 stand for the first and second measurement at a single point in the flow field, separated by δt_2.

$$R_{u_1 u_2} = \frac{\overline{u'_1 u'_2}}{\sigma_{u_1} \sigma_{u_2}} \tag{1}$$

This correlation coefficient may be interpreted as a measure for the duration of coherence of a flow phenomenon at fixed spatial coordinates. One can think of observing the passage of a vortical structure in the incoming boundary layer from a stationary point in space. For small very small δt_2 (i.e., much smaller that the passing time of the vortex) the passing flow structure will hardly have moved and a very high correlation coefficient is obtained. For increasingly large δt_2 the vortex will displace over a larger distance and the correlation coefficient will decrease accordingly, until the vortex has moved out of sight and hence the correlation vanishes. The same reasoning can be applied to other flow features as well. Low frequency phenomena or long wave length flow structures will lead to higher values of the correlation coefficient at large δt_2.

An effect that has to be taken into account is the slow time drift in the free-stream velocity inherent to blow down facilities as a consequence of the transient total temperature condition in the supply vessel (see section II). The effect on the mean velocity is inferior to the free-stream turbulence and the measurement uncertainty. Nonetheless, a velocity trend does constitute a coherent very low frequency flow motion. A similar, additional low frequent motion due to this velocity trend is introduced as a consequence of the discontinuities when combining multiple runs to compute the correlation statistics. This would result in a residual non-zero value of the correlation coefficient at

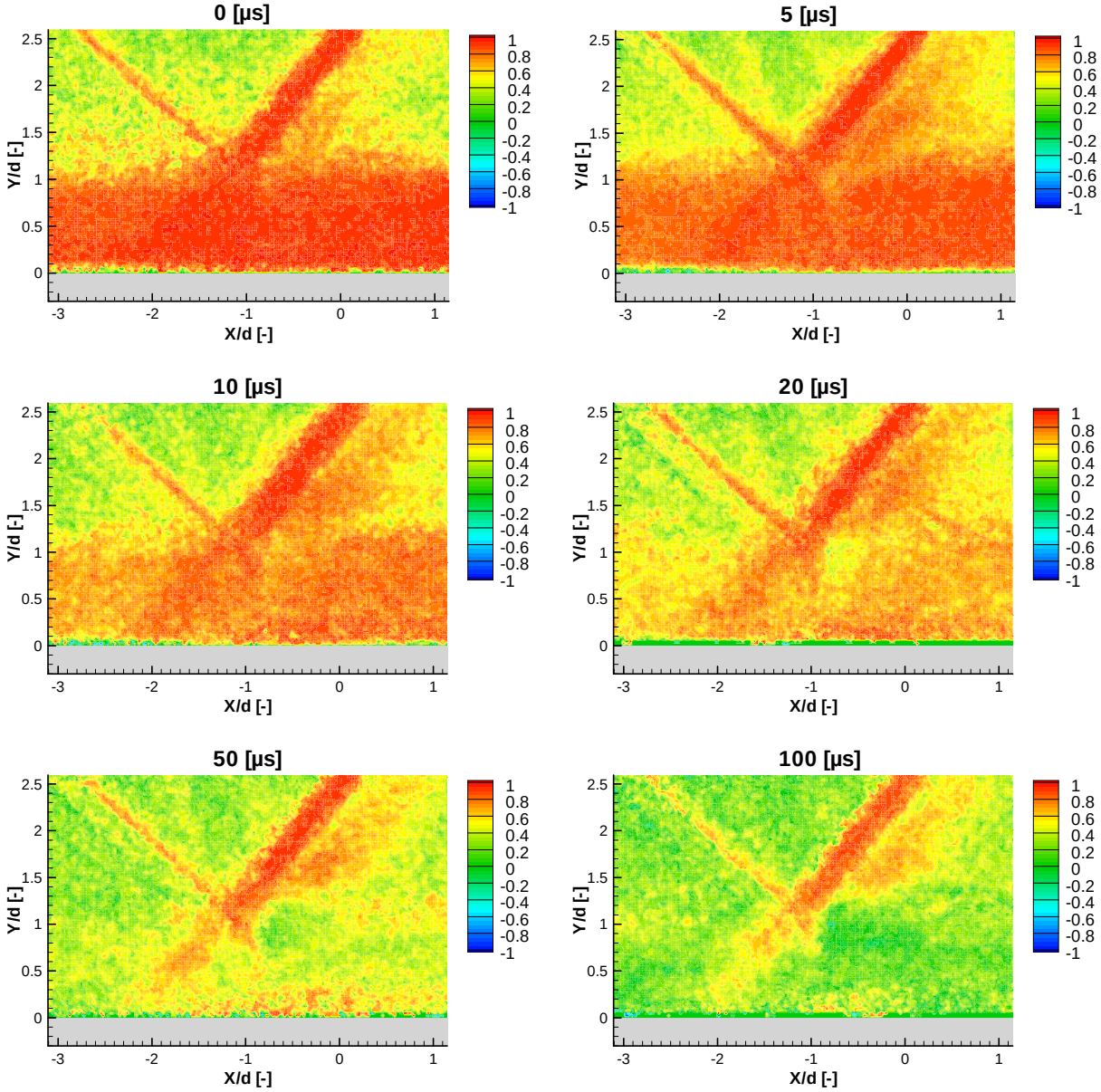

Figure 9. The temporal auto-correlation coefficient for small time delays.

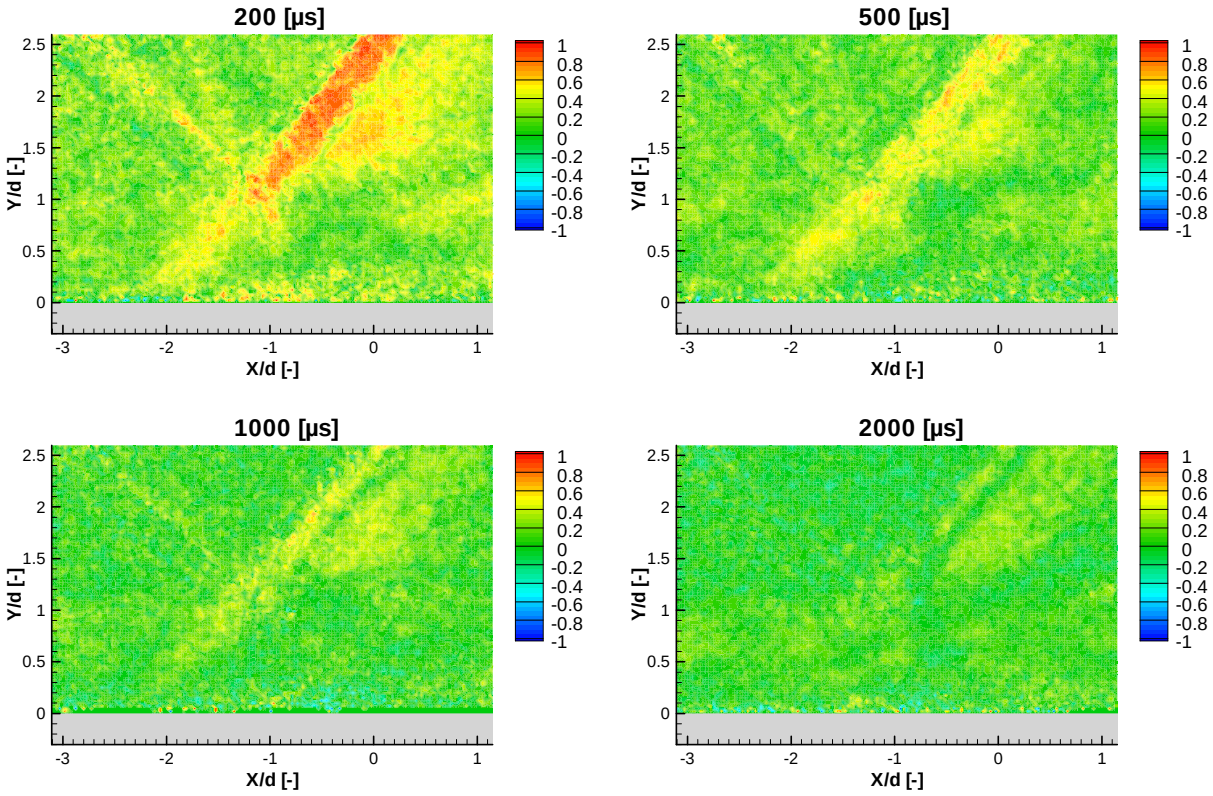

Figure 10. The time correlation coefficient for large time delays.

large δt_2. To remedy this, the velocity data have been corrected for any linear trends. The time correlation statistics have consecutively been computed for the correctly zero mean centred velocity fluctuations.

In the first place it is observed that for δt_2=0 µs, where both measurements should be identical and thus have a correlation coefficient of unity, not all of the flow is fully correlated. Especially in the external flow, where the fluctuations are small, the correlation is medium to low. This may be attributed to measurement noise and may indeed be interpreted as a measure of the accuracy of the PIV technique. As a second remark, it may be noticed that the incident shock wave appears in the correlation results for small δt_2. Since the incident shock was verified to be steady and since it appears for the zero-time-delay case as well, also this feature may be attributed to limitations inherent to the PIV measurements technique close to the shock, as in the case of the fluctuation statistics and the Reynolds stress.

A qualitative evaluation of the correlation coefficient in figure 9 and figure 10 shows that for small δt_2 below 10 µs all regions of interest (the incoming boundary layer, the interaction zone and the reflected shock in combination with the expansion fan) remain highly correlated with values close to unity. Evidently, on the scale of the measurement resolution, no flow regions display time scales that are substantially below 5 µs, justifying the choice of this time delay as the smallest value in the investigation. The incoming boundary layer is the first region to decorrelate, starting from δt_2=10 µs. The boundary layer is largely decorrelated at δt_2=50 µs. At this time delay the interaction zone with the mixing layer and the subsequent vortex shedding and recovering boundary layer are still correlated. Somewhere between δt_2=100 µs and 500 µs, the mixing layer and vortex shedding regions also become decorrelated. The reflected shock shows high values of the correlation coefficient throughout most of the range of time delays considered so far. Only for the very large time delays does it start to decorrelate. The correlation coefficient of the reflected shock has practically vanished at δt_2=2000 µs. This confirms the existence of different time scales within the flow domain, and in particular it evidences the low frequency behaviour of the reflected shock.

This qualitative evaluation of the time scales can be quantified further by plotting the local time correlation coefficient against the time delay for different locations in the flow, see figure 11. The selected regions of interest are shown in the top of this figure (superimposed on the auto-correlation coefficient at δt_2=200 µs and contours of the Reynolds stresses for reference; the dashed horizontal line indicates the approximate edge of the undisturbed

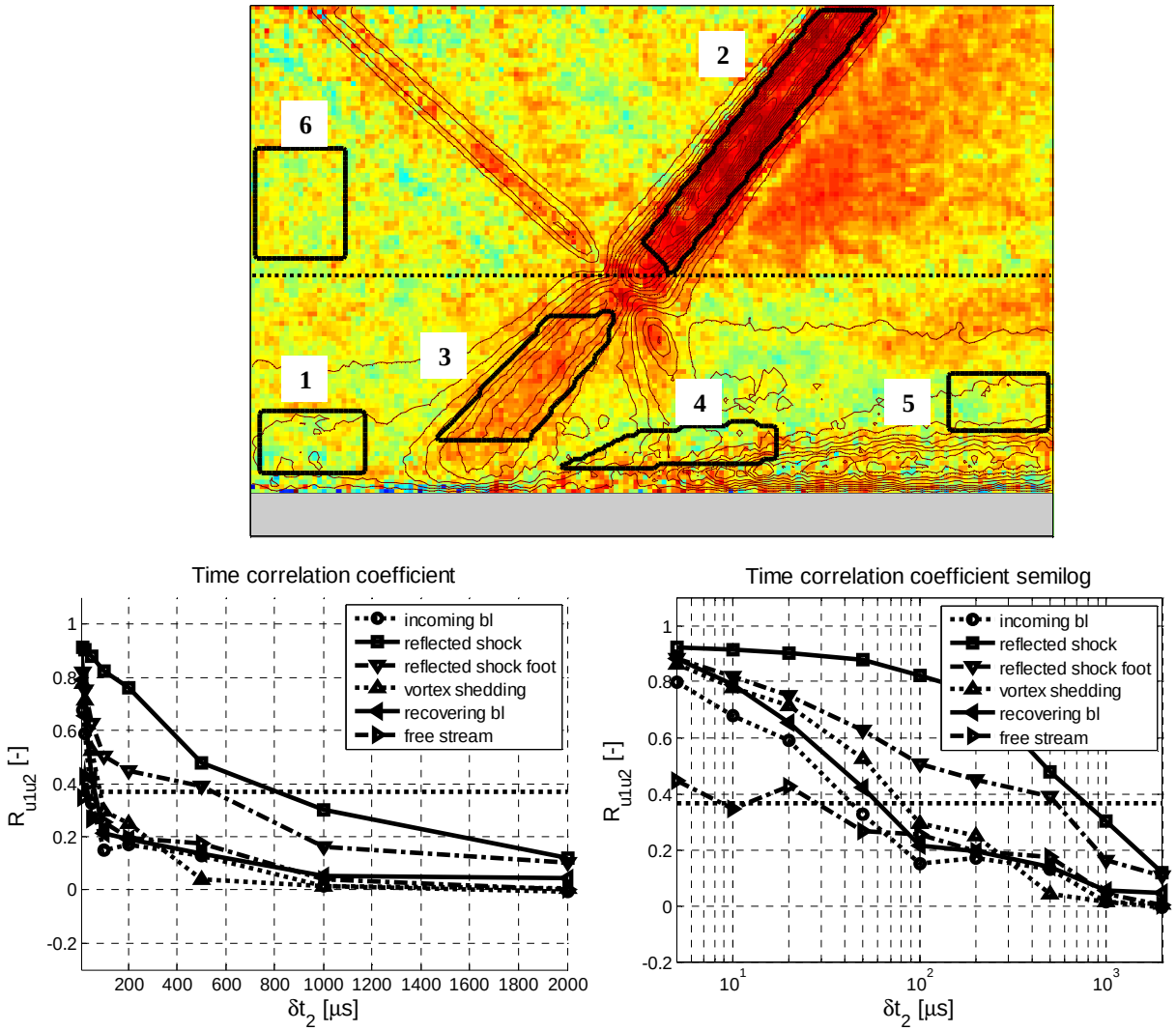

Figure 11. Local temporal auto-correlation coefficient for selected regions of the flow field. Top: regions under consideration (1: incoming boundary layer, 2: reflected shock, 3: reflected shock foot, 4: vortex shedding, 5: recovering boundary layer, 6: free stream). Bottom-left: auto-correlation coefficient for each respective region. Bottom-right: auto-correlation coefficient in semi-log representation.

boundary layer). Statistics have been computed over multiple points within each region of the flow to aid the statistical convergence (note that only 200 realisations are available per time delay). The fluctuations in each point are centred locally around a zero mean value by means of the aforementioned detrend routine. The correlation statistics are computed consecutively, treating the combination of points as a single data ensemble while taking into account the proper weighting for rejected vectors. It has been verified that no significant dependence of the results exists on the selection of each region within the local flow domain under consideration. For reference, the auto-correlation coefficient in the free-stream is also shown. The results have been plotted in both linear and semi-log representation, the latter to better visualise the different orders of magnitude of the time scales.

The different orders of magnitude are clearly apparent from figure 11. The auto-correlation coefficients of the reflected shock have not yet vanished for the large time delays, while the values of the other regions have already converged asymptotically to zero at approximately δt_2=1000 µs. Taking the crossing of the 1/e-level of the auto-correlation coefficient as representative for the time scales, it is evident that the smallest time scales are found in the incoming boundary layer, followed by the recovering boundary layer, the vortex shedding, the reflected shock foot and the reflected shock. Looking at the incoming boundary layer, a characteristic time is obtained of 40 µs and hence a frequency of 25 kHz. Considering an integral length scale of Λ/δ = 0.5 (see Ref. 6) and a convective

velocity of $0.8U_e$ yields an integral time scale of 24 µs and hence a frequency of 42 kHz. The boundary layer time scales hence appear to be over-estimated. It is unknown if this over-estimated value is physical or whether it is a measurement artefact. As for the vortex shedding, a characteristic time scale of 80 µs is obtained, corresponding to 12.5 kHz. For the reflected shock, a time scale of 800 µs, or 1250 Hz, is obtained. Both the measured frequency of the vortex shedding and the one of the reflected shock are of approximately the same order of magnitude as the values observed in literature (see Ref. 3).

Considering figure 11 further, two interesting observations can be made. In the first place, the reflected shock foot, the vortex shedding and the recovering boundary layer regions all show the same behaviour for small time delays, and further follow more loosely the trend of the incoming boundary layer. For larger time delays, the downstream boundary layer seems to tend towards the incoming boundary layer, diverging from the vortex shedding trend. This is indeed indicative of the recovery process of the boundary layer. For larger time delays, the incoming boundary layer, the vortex shedding and the recovering boundary layer curves are more difficult to interpret since they become of the same order of magnitude as the free-stream value, i.e. essentially loosing correlation. It is noted however that the auto-correlation value itself in the free-stream is very small (one to two orders of magnitude smaller in comparison to the other regions).

A second important observation is that the reflected shock foot auto-correlation coefficient displays a behaviour intermediate to the incoming boundary layer and the reflected shock in the outer flow. At small time delays, the reflected shock foot responds rather similar to the incoming boundary layer while at larger time delays the reflected shock foot seems to behave like the reflected shock in the external flow. Hence, even though the signal is influenced by the passage of turbulent structures present in the incoming boundary layer, there is also a strong low frequency component. This indicates that the reflected shock foot moves in harmony with the low frequency motion of shock in the outer flow. A similar behaviour has indeed been observed in LES simulations of this kind of interactions[17].

Conclusion

A Dual-PIV approach was used to study time-correlation phenomena in a shock-wave boundary layer interaction over a large range of time scales, including small values of the time delay that are not achievable by a single PIV-system (max. equivalent repetition rate 200 kHz) The Dual-PIV measurements have been validated with respect to classical two component PIV measurement and with respect to semi-empirical relations for the friction coefficient and the friction velocity. In a statistical sense, the measurements of the incoming boundary layer and the interaction were found to be in agreement with the previous PIV measurements. No dependence on the measurement resolution was observed of the mean velocity, the fluctuation statistics and the Reynolds stress (except for the last points close to the wall, which are not accessible with PIV). The mean velocity and the u-component fluctuations are well resolved down to y/δ=0.1. It is concluded that the flow under consideration is in accordance with previous measurements and that the results are of consistent quality.

Dual-PIV has been used to classify the time scales in the shock wave boundary layer interaction. This classification has shown that the time scales span three orders of magnitude. The smallest time scales are present in the incoming boundary layer. The obtained frequency of 42 kHz seems to be over-estimated with respect to the expected integral times scales. It is not known whether this is physical or a measurement artifact. The frequencies for the vortex shedding and the reflected shock, 12.5 kHz and 1250 Hz respectively, seem to be in accordance with literature. The low frequency motion of the reflected shock has been confirmed.

The auto-correlation coefficient of the downstream boundary layer region follows the vortex shedding trend for small time delays and converges towards the incoming boundary layer values for medium time delays. This could be indicative of the recovery of the boundary layer after the interaction. Finally, the results indicate that the shock foot moves in harmony with the low frequency motion of shock in the outer flow.

Acknowledgments

The current research was supported by the European Commission in the context of the 6th Framework Programme UFAST “Unsteady effects in shock induced separation” (www.ufast.gda.pl). This work constitutes a cooperation between the Delft University of Technology (TU Delft) and the Groupe Supersonique of the IUSTI (UMR CNRS 6595) in Marseille. The experiments were performed at the TU Delft and the majority of the data processing took place at the IUSTI. The author wishes to gratefully acknowledge the input, ideas and support of both institutions.

References

[1]Cousteix, J., *Turbulence et couche limite*, CEPADUE-Editions, Toulouse, 1989.

[2]Dolling, D.S., "Fifty Years of Shock-Wave/Boundary-Layer Interaction Research: What Next?," *AIAA Journal*, Vol. 39, No. 8, Aug. 2001, pp. 1517-1531.

[3]Dupont, P., Haddad, C., Debiève, J.-F., "Space and time organisation of a shock-induced separated boundary layer," *Journal of Fluid Mechanics*, Vol. 559, 2006, pp. 255-277.

[4]Dupont, P., Piponniau, S., Sidorenko, A., Debiève, J.-F., "Investigation of an Oblique Shock Reflection with Separation by PIV Measurements," *AIAA Aerospace Science Meeting and Exhibit*, 8-11 Jan. 2007, Reno, Nevada (USA)

[5]Dussauge, J.P., Dupont, P., Debiève, J.-F. "Unsteadiness in Shock Wave Turbulent Boundary Layer Interactions with Separations," *Aerospace Science and Technology*, Vol. 10, 2006, pp. 85-91.

[6]Dussauge, J.P., and Smits, A.J., "Characteristic scales for energetic eddies in turbulent supersonic boundary layers," *Proceedings of the Tenth Symposium on Turbulent Shear Flows*, Pensylvania State University, 1995.

[7]Elsinga, G.E., Van Oudheusden, B.W., Scarano, F. "Evaluation of optical distortion effects in PIV," *Experiments in Fluids*, Vol. 39, 2005, pp. 246–256.

[8]Fernholz, H., "Ein halbempirisches Gesetz für die Wandreibung in kompressiblen turbulenten Grenzschichten bei isothermer und adiabater Wand," *Angewandte Mechanik*, ZAMM 51, 1971, T 146-147.

[9]Ganapathisubramani, G., Clemens, N.T., Dolling, D.S. "High-speed PIV measurements to study the effect of upstream coherent structures on shock-induced turbulent separation," *7th International Symposium on Particle Image Velocimetry*, 11-14 Sep. 2007, Rome, Italy.

[10]Humble, R.A., Scarano, F., Van Oudheusden, B.W., "Experimental study of an unsteady impinging shockwave/turbulent boundary layer interaction using PIV," *36th AIAA Fluid Dynamics Conference and Exhibit*, 5-8 Jun. 2006, San Francisco, USA, AIAA Paper 2006-3361.

[11]Liu, X., Katz, J. "Instantaneous pressure and material acceleration measurements using a four-exposure PIV system," *Experiments in Fluids*, 2006, DOI: 10.1007/s00348-006-0152-7.

[12]Perret, L., Braud, P., Fourmet, C., David, L., Delville, J. "3-Component acceleration field measurement by dual-time stereoscopic particle image velocimetry," *Experiments in Fluids*, Vol. 40, 2006, pp. 813-824.

[13]Scarano, F., Riethmuller, M.L., "Iterative multigrid approach in PIV image processing with discrete window offset," *Experiments in Fluids*, Vol. 26, 1999, pp. 513-523.

[14]Smits, A.J., Dussauge, J.P., *Turbulent Shear Layers in Supersonic Flow*. 2nd ed., Springer, New York, 2006.

[15]Souverein, L.J., Van Oudheusden, B.W., Scarano, F., "Particle image velocimetry based loads determination in supersonic flows," *45th AIAA Aerospace Sciences Meeting and Exhibit*, 8-11 Jan. 2007, Reno, Nevada, USA, AIAA Paper 2007-0050.

[16]Souverein, L.J., Van Oudheusden, B.W., Scarano, F., "Determination of time scales in a Shock Wave Turbulent Boundary Layer Interaction by means of Dual PIV," *7th International Symposium on Particle Image Velocimetry*, 11-14 Sep. 2007, Rome, Italy.

[17]Touber, E., Sandham, N.D., "Oblique Shock Impinging on a Turbulent Boundary Layer: Low-Frequency Mechanisms," *38th AIAA Fluid Dynamics Conference*, 23–26 June, Seattle, USA, AIAA Paper 2008-4170.

[18]Van Oudheusden, B.W., Scarano, F., Roosenboom, E.W.M., Casimiri, E.W.F., Souverein, L.J., "Evaluation of integral forces and pressure fields from planar velocimetry data for incompressible and compressible flows", *14th Int. Symp. on Applications of Laser Techniques to Fluid Mechanics*, 26-29 Jun. 2006, Lisbon, Portugal. Final paper published in: *Experiments in Fluids*, 2007 DOI: 10.1007/s00348-007-0261-y.

[19]Van Oudheusden, B.W., Souverein, L.J., "Evaluation of the pressure field from PIV in a shock wave boundary layer interaction", *7th International Symposium on Particle Image Velocimetry*, 11-14 Sep. 2007, Rome, Italy.